China Geology 6 (2023) 241−251

China Geology

Journal homepage: http://chinageology.cgs.cn
https://www.sciencedirect.com/journal/china-geology

The first discovery of Xinlong epithermal gold deposit in southern margin of the Bangonghu-Nujiang metallogenic belt: A new expansion of gold prospecting in Northern Tibet

Wei Chen[a,*], Yang Song[a], Qing-ping Liu[b], Miao Sun[b], Jia-jia Yu[a], Yang Li[b], Qi Zhang[b], Chang Liu[b]

[a] *MNR Laboratory of Metallogeny and Mineral Assessment, Institute of Mineral Resources, Chinese Academy of Geological Sciences, Beijing* 100037, *China*
[b] *School of Earth Science and Resource, China University of Geosciences (Beijing), Beijing* 100083, *China*

ARTICLE INFO

Article history:
Received 13 January 2023
Received in revised form 13 April 2023
Accepted 14 April 2023
Available online 18 April 2023

Keywords:
Epithermal gold deposit
Xinlong gold deposit
Central Lhasa subterrane
Bangonghu-Nujiang metallogenic belt
Mineral exploration engineering
Tibet

ABSTRACT

The Xinlong gold deposit is located in Niyma County, Naqu area of Tibet and was discovered by the Institute of Mineral Resources, Chinese Academy of Geological Sciences through the 1∶50000 mineral geological survey. The ore bodies occur in the Zenong Group volcanic rocks in the middle section of the central Lhasa subterrane and are structurally controlled by the NNW-striking faults. Four ore bodies have been found, exhibiting cloddy, dense-sparse, disseminated, and breccia structures. The ore minerals are mainly tetrahedrite group minerals, and other ore minerals include pyrite, chalcopyrite, nevskite, bornite, anglesite, native gold, and silver-gold bearing selenide, etc. The types of alteration are dominated by silicification, as well as middle- and high-graded argillization. The alteration mineral assemblages contain quartz, pyrophyllite, and kaolinite. The Zaliela Formation volcanic rocks of Zenong Group are silicified by later hydrothermal fluid with vuggy quartz in some fractured zones. The middle- and high-graded argillization are characterized by pyrophyllitization and kaolinization. The Xinlong gold deposit shows great metallogenetic potentiality and has been revealed by 1∶10000 geological mapping, IP sounding, and trial trenching in the mining area. Combined with the regional metallogenic geological setting, we suppose that a potential epithermal gold belt probably exists in the middle of the Lhasa terrane. The discovery of the Xinlong gold deposit opens a new chapter for the gold prospecting in Northern Tibet.

1. Introduction

The Qinghai-Tibet Plateau is well known for its abundant placer gold. Since the discovery of the Bengnazangbu placer gold deposit in 1918, the placer gold deposits in Tibet have been exploited for more than a hundred years. The long history of gold panning and prospecting indicates a great potential for gold prospecting (Tang JX et al., 2017). Two gold mineralized zones have developed in the south and the north of the central Qinghai-Tibet Plateau between the Bangong-Nujiang Suture Zone (BNSZ) and the Luobadui-Milashan fault. The northern gold mineralized zone is mainly distributed along the BNSZ, with gold occurring mainly along the northern margin of the Bangonghu-Nujiang ophiolitic melange zone. The major gold deposits in this mineralized zone include Shangxu, Laga, Dacha, Nama, Zensewu, Suoqu, Buqule, Zayihuima, Tangza, Xiyalong, Sangong, Lama, and Galigou (Fig. 1, Huang HX et al., 2014; Fang X et al., 2020a, 2020b, 2020c). The southern gold mineralized zone is primarily located in the central part of the central Lhasa terrane (the Longeer-Nyainqentanglha composite paleo-island arc belt). This zone hosts the largest Bengnazangbu placer gold deposit in Tibet, with placer gold reserves of more than 13 t (Wang CH et al., 2006). The other gold ore occurrences/mineralized points are also widely distributed in the Qinghai-Tibet Plateau, including Zhongnong, Zhenongla, Sunna, Genong, Jinongyan, Sebula, Chaouqiong, Tiangongnile, Gegacun, Songduo, Zhigeima and Bangzhuo. In addition, there are many unknown placer gold deposits scattered throughout the area, which however are dominated by small-scale ore occurrences/mineralized points. So far, no large-scale rock gold deposit has been discovered in Northern Tibet, and no breakthrough has been made in gold prospecting

* Corresponding author: *E-mail address*: nmgchenwei@163.com (Wei Chen).

Literary editor: Xi-jie Chen
doi:10.31035/cg2023011
2096-5192/© 2023 China Geology Editorial Office.

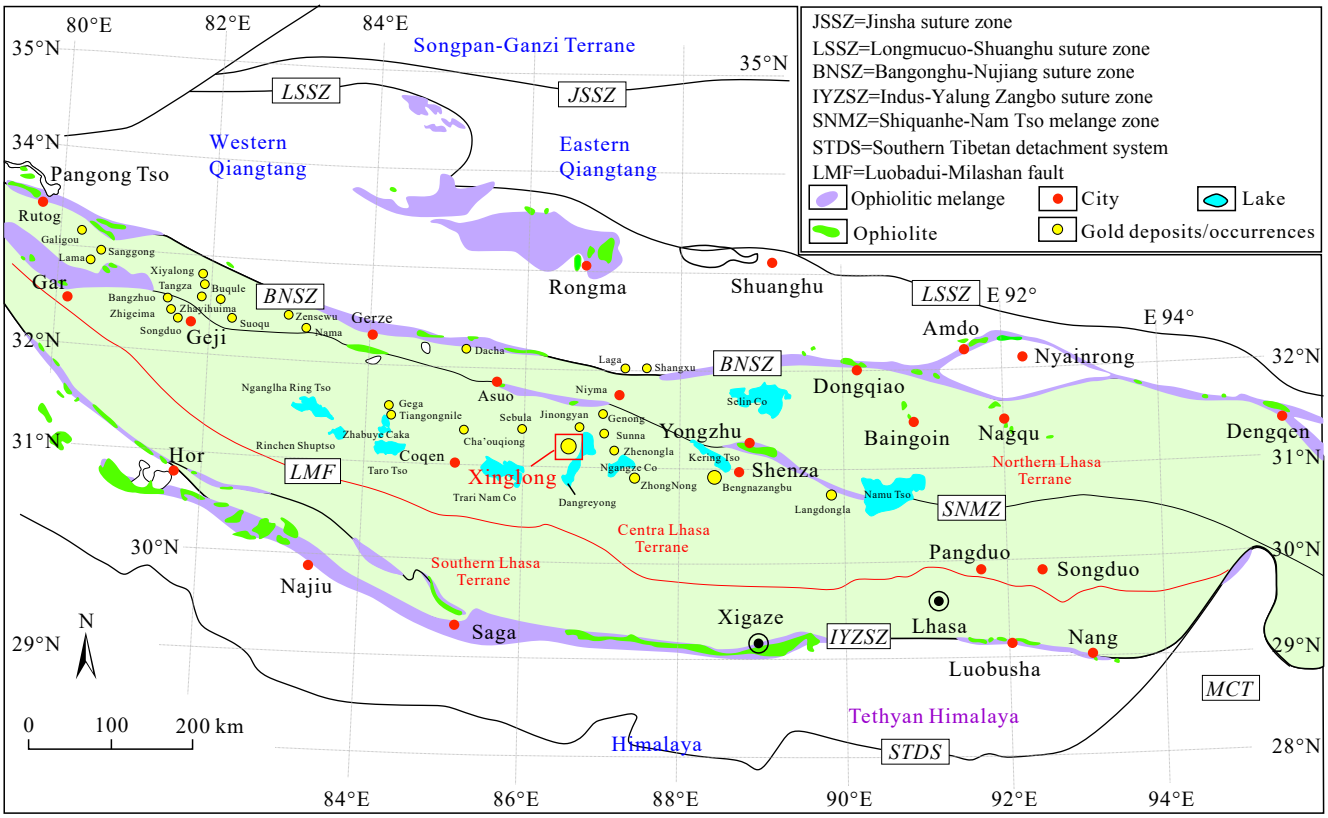

Fig. 1. Distribution of the ore occurrences of rock gold on the southern margin of the Bangonghu-Nujiang metallogenic belt (modified from Zhu DC et al., 2016).

in this area.

The vast Qinghai-Tibet Plateau is an important part of the Tethys Ocean tectonic system, characterized by the development of the Paleo-, Meso- and Neo-Tethys oceans (Gehrels G et al., 2011). It has experienced a complex geological history that includes the subduction and extinction of the Tethys Ocean, the collision between the Lhasa and Qiangtang terranes, and the collision and extension between the Asian and Indian continents. Large-scale tectonic-magmatic activities continued from the Late Triassic to the Neogene (Tang JX et al., 2014). Tang JX et al. (2012) summarized the metallogenic series and regional metallogenic lineages of the Gangdise metallogenic belt, the Bangonghu-Nujiang metallogenic belt, and the Himalayan metallogenic belt in northern and southern Tibet according to a series of metallogenic theories of deposits. They proposed that the most promising metallogenic series of epithermal porphyry copper-gold deposits in Tibet include the metallogenic subseries of copper, gold, silver, and lead-zinc deposits associated with the Early Cretaceous island-arc intermediate-felsic rocks in the Bangonghu-Nujiang metallogenic belt and those associated with the Early-Late Jurassic island-arc intermediate-felsic rocks in the Gangdise metallogenic belt. On this basis, during the performance of the comprehensive exploration and assessment project of the copper-polymetallic resource base in northwest Tibet organized by the Institute of Mineral Resources under the Chinese Academy of Geological Sciences, the project team conducted a 1∶50000 scale mineralogical and geological survey in the western Tangra Yumco area of Nyima County in Tibet and discovered the Xinlong gold deposit during 2020–2021 (Chen W et al., 2022a, 2022b). This deposit has exposed large-scale ore bodies, a high ore grade, and great metallogenic potential. The discovery of the Xinlong gold deposit indicates that continental volcanic rocks in the Northern Tibet have potential to explore epithermal gold deposit.

2. Regional geological setting

With a better understanding of the ocean's evolution, the bidirectional subduction of the Banggai-Nujiang Ocean has been accepted in recent years (Qu XM et al., 2012; Zhu DC et al., 2016). In a narrow sense, the Bangonghu-Nujiang metallogenic belt includes only the ophiolitic melange belt in the suture line. In general, this metallogenic belt contains–in addition to the ophiolitic melange belt in the suture line–magmatic rock areas on the north and south sides of the suture line that were formed by the subduction, collision, post-collision, and intracontinental extension of the Bangong-Nujiang Ocean (Geng QR et al., 2013; Song Y et al., 2014). Therefore, the Bangonghu-Nujiang metallogenic belt is located between the Longmuco-Shuanghu ophiolitic melange belt and the Luobadui-Milashan fault (Fig. 1). It covers the southern margin of the southern Qiangtang terrane, the BNSZ, and part of the north-central Lhasa terrane, with a west-east extension of more than 2000 km and an area of about 490000 km^2 (Song Y et al., 2014). The Xinlong gold deposit is located at the southern margin of the Bangonghu-Nujiang

metallogenic belt and in the central part of the central Lhasa terrane (Fig. 1). In the central Lhasa terrane, the magmatic rocks in the north-central part include mainly the volcanic rocks of the Late Jurassic-Early Cretaceous Zenong Group (Zhu DC et al., 2008), while the magmatic rocks in the south-central part mainly include the volcanic rocks of the Paleocene-Late Eocene Linzizong Group (Ma XX et al., 2020). The central part of the central Lhasa terrane is covered by the EW-trending Longeer-Nyainqentanglha fault zone, where Paleozoic strata are primarily exposed, including the Carboniferous Yongzhu Formation, the Late Carboniferous-Early Permian Laga Formation, and the Late Permian Xiala Formation. This fault-uplift zone occurs intermittently and is partially displaced or covered by the late-stage SN-trending rifts or volcanic rocks. The southern gold mineralized zone on the central Qinghai-Tibet Plateau is mainly distributed along this fault-uplift zone.

3. Geological characteristics of the Xinlong deposit

3.1. Geological setting of the mining area

The geological bodies exposed in the mining area of the Xinlong gold deposit mainly include the Late Paleozoic Laga and Angjie formations and the volcanic rocks of the Zaliena Formation of the Early Cretaceous Zenong Group (Fig. 2). The Laga Formation is mainly distributed in the north-central part of the mining area. It is composed of grayish black-dark gray siltstones interbedded with fine-grained sandstones and conglomeratic siltstones, and all of these rocks are generally subjected to limonite alteration (Figs. 3a–c). The Angjie Formation, which is primarily distributed in the southeastern part of the mining area, consists of a set of rock assemblages of argillaceous siltstones interbedded with limestones. The volcanic rocks of the Zaliena Formation of the Zenong Group are distributed in the southwest and southeast of the mining area. They are a set of rock assemblages consisting of andesitic, dacitic, and rhyolitic lavas and corresponding pyroclastic rocks, with silicification and limonite alteration widely distributed (Figs. 3a–d). These volcanic rocks unconformably overlie the fine cuttings of the Laga Formation and are the main ore-bearing strata in the mining area. A set of granite porphyries are exposed in the northeast of the mining area, emplacing the Laga Formation in the form of small stocks. A nearly EW-trending fault (F1) has developed in the mining area, and the EW is the primary structural direction in the mining area. Moreover, the NNW-trending faults (F3, F4, F5 and F6) are the main ore-controlling structures in the mining area. The structures occurring in the mining area create favorable conditions for gold mineralization (Fig. 2).

3.2. Geological characteristics of the ore bodies

The ore bodies in the mining area of the Xinlong gold deposit occur mainly in the NNW-trending tectonically fractured zone in the volcanic rocks of the Zenong Group (Fig. 2). They are dominated by strongly silicified, tectonically altered rocks that show strong malachite alteration at the surface (Figs. 4a–d). During the 1∶10000 geological mapping, 11 mineralized outcrops were discovered in the mining area and labeled as Au-Cu mineralized outcrops 1–11 (Fig. 2). Among them, Au-Cu mineralized outcrops 1–2 are controlled by faults F3 and F4 and are ore bodies I and II, respectively. Au-Cu mineralized outcrops 3–8 are controlled by fault F5 and collectively form ore body III–the main orebody in the mining area. Au-Cu mineralized outcrop 11 is controlled by fault F6 and is orebody IV according to the induced polarization (IP) sounding, which also reveals that Au-Cu mineralized outcrops 9–10 may be controlled by the secondary fault of F6. The outcrops of ore body I have a width of about 5 m and a length of 300 m (Fig. 4b). The outcrops of ore body II have a width of about 8–10 m. With a cut-off grade of 0.5 g/t and a minimum band rejected thickness of 2 m as boundary conditions, ore body II extends for 450 m northwestward, with an average width of 8.33 m and an average gold grade of 2.21 g/t, as indicated by three exploratory trenches. Ore body II has predicted prospective resources of about 3.28 t (Chen W et al., 2022a).

As the main ore body in the mining area, ore body III occurs in an intermittently bead-like form along fault F5, with a width of 6–18 m and a length of 800 m. The mineralization in the mining area tends to intensify significantly from ore bodies I and II in the southwest to ore body III in the center. The mineralization assemblages of ore body II in the southwest of the mining area are dominated by quartz, a small amount of pyrite, and a small amount of chalcopyrite, indicating a low gold grade. In contrast, the mineralization assemblages of ore body III at the top of the mountain in the central mining area are dominated by quartz and tetrahedrite, resulting in a much higher gold grade. For instance, the surface samples from Au-Cu mineralized outcrop 7 had a gold grade of up to a maximum of 90.5 g/t. Other mineralized outcrops of ore body III also have relatively high grades of gold (Au), and 23 surface samples had an average Au grade of up to 15.06 g/t. In addition to Au, ore body III is also associated with other useful elements such as Ag, Cu, and Sb, all of which have high grades. For instance, 29 samples had an average Ag grade of up to 307.5 g/t.

As shown by the IP sounding results, there is a high-resistivity and high-polarizability anomalous body with an extended depth of more than 250 m and a width of more than 120 m in the lower part of ore body III. This anomalous body has physical properties that are consistent with those of silicified altered rocks containing metal sulfides. Therefore, it can be inferred that a huge ore body exists in the lower part of ore body III. As shown by the pseudosection of electric polarizability (ηs) isolines obtained by IP sounding, the polarizability increases significantly in the lower part, with ηs increasing from 0.3% at the surface to 2.9%. This result indicates that the number of metal ions increases significantly in the lower part and thus the ore grade could be much higher. Despite the insufficient surveys to date, the prospective resources of the ore body III are expected to reach a large

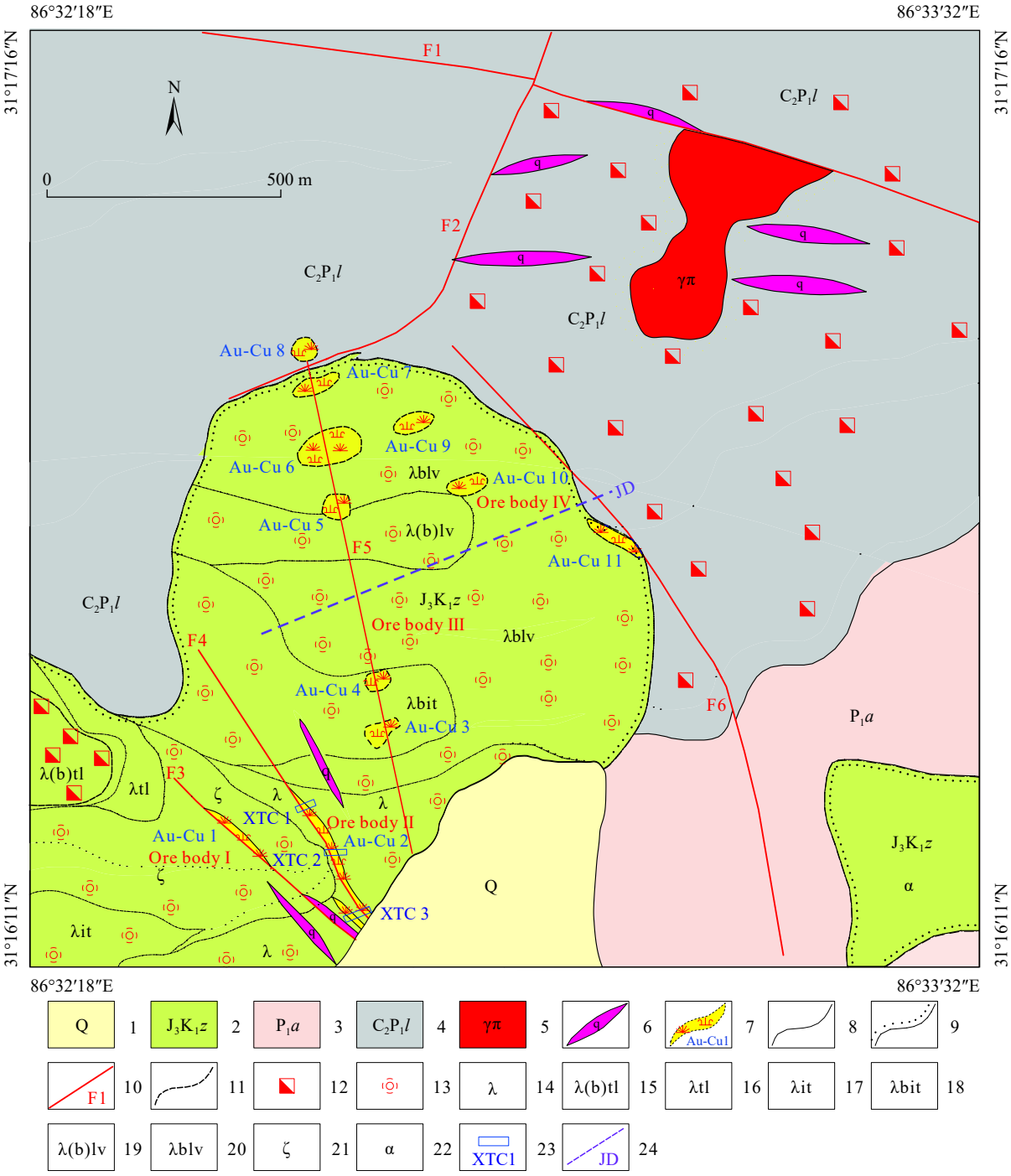

Fig. 2. Geological map of the Xinlong gold deposit (modified from Chen W et al. 2022b). 1–Quaternary; 2–Upper Jurassic-Lower Cretaceous Zalena Formation; 3–Lower Cretaceous Angjie Formation; 4–Upper Carboniferous-Lower Permian Laga Formation; 5–Granite porphyry; 6–Quartz vein; 7–Au and Cu mineralized zone and number; 8–Geological boundary; 9–Angular unconformity boundary; 10–Fault; 11–Lithofacies boundary; 12–Ferritization; 13–Silicification; 14–Rhyolite; 15–Rhyolitic pebbly tuff lava; 16–Rhyolitic tuff lava; 17–Rhyolitic fused tuff; 18–Rhyolitic breccia fused tuff; 19–Rhyolitic pebbly lava; 20–Rhyolitic breccia lava; 21–Dacite; 22–Andesite; 23–Trial trench and number; 24–IP sounding profile.

scale or even a super-large scale based on the extent of the outcrop scale, the ore grade of the surface samples, and the depth of the ore body as determined by geophysical analysis. Ore body IV is largely buried, with only weak Au-Cu mineralization 11 exposed on the surface. The IP sounding results show that significant anomalies with high resistivity and high polarizability exist 20 m below the surface. This result indicates that a high-grade ore body may be present in the lower part, and the specific resources need to be verified by further drilling (Chen W et al., 2022b). In summary, the Xinlong gold deposit has a great metallogenic prospect and the potential for prospecting.

3.3. Alteration characteristics

The samples were mainly collected from outcrops of the

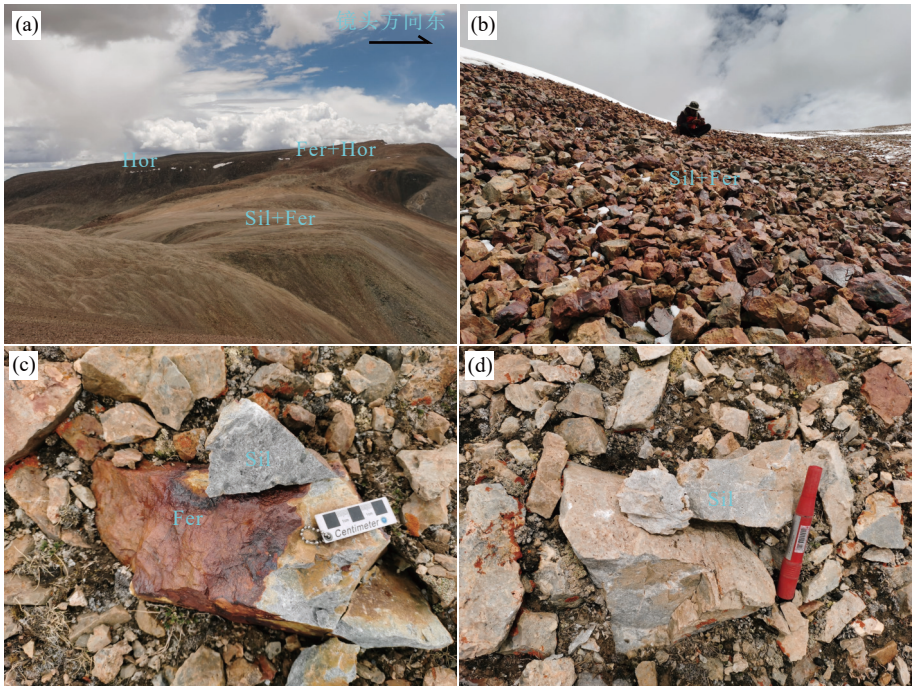

Fig. 3. Macroscopic alteration photos of the mining area. Silicitization, ferritization and hornfelsization are developed in the Xinlong mining area (a), silicitization and ferritization are developed in the Zenong Group volcanic in the north part of study area (b), strong silicitization and ferritization are developed in the Zenong Group volcanic in the Southwest part of the Xinlong mining area (c) and typical silicified rocks (d). Sil–silicification; Fer–ferritization; Hor–hornfelsization.

No. II and No. III ore body. As shown by systematic on-site sampling and detailed microscopic identification, spectral scanning, and electron probe microanalysis (EPMA), the alternation of the surface ore bodies is dominated by silicification, followed by intermediate to high-grade argillization (Table 1). As the dominant alteration in the mining area of the Xinlong gold deposit, silicification (i.e., secondary quartzification) occurs on a large scale in the southwest of the mining area (Figs. 3a–d). As the surrounding rocks, the volcanic rocks of the Zaliela Formation of the Zenong Group were metasomatized by late volcanic hydrothermal fluids and then silicified, forming altered rocks and leading to the widespread occurrence of vuggy quartz (Figs. 4e–g, 5a–e).

The argillization is present mainly in the form of pyrophyllite and kaolinite alteration. Pyrophyllites occur locally and are waxy white in color (Fig. 4h). Under the microscope, the pyrophyllites are tiny, long lamellar aggregates that show three-level bright interference colors (Figs. 5d–f). The kaolinites occur mainly in brecciated ores. They are in the form of milky-white lumps and exhibit an earthy luster (Figs. 4i–j). Under a polarized-light transmission microscope, kaolinites are colorless or yellowish and are in the form of tiny flakes, often forming flaky, superimposed aggregates (Fig. 5g). With the exception of the K-bearing kaolinites and a part of the pyrophyllites, most of the altered minerals are K-bearing aluminosilicates, which have significantly higher K content than the pyrophyllites but much lower K content than mica minerals and are thus inferred to be sericites that are not subjected to complete pyrophyllite alteration (Fig. 5f). In summary, the alteration mineral assemblages consist of silicification and intermediate to high-grade argillization and have similar characteristics to the intermediate to high-grade argillization at the periphery of high-sulfidation epithermal deposits (Hedenquist JW et al., 2000).

3.4. Ore characteristics

The mineralization in the mining area can be preliminarily divided into three stages: the first stage of quartz-pyrite-chalcopyrite alteration, the second stage of quartz-tetrahedrite, and the third stage of quartz-nevskite-naumannite-native gold metallogenic (which is the main metallogenic stage).

The quartz-pyrite-chalcopyrite stage is the early mineralization of the Xinlong gold deposit. The quartz, pyrite, and chalcopyrite formed at this stage mainly occur in southwestern ore bodies I and II, which are far from the mineralization center of the mining area. A large amount of porous quartz has developed in the ores (Figs. 4e–g, 5a–c). The metallic mineral assemblages formed in this stage mainly consist of pyrite and chalcopyrite, which are sparsely disseminated and commonly formed in the vugs of the vuggy quartz (Figs. 4f–g, 5b–c). Based on the exploration trenches, it has been determined that ore body II has a maximum ore grade of 6.95 g/t and an average ore grade of 2.15 g/t. Under the microscope, the pyrite is yellowish-white and subhedral or anhedral and has a wide grain size range from tens of microns to several millimeters, with the majority being microfine-grained (Figs. 5c, h). In contrast, the chalcopyrite is brassy yellow and irregularly granular and has the same grain size range as the pyrite (Fig. 5c).

The quartz and tetrahedrite formed at the second stage,

Fig. 4. Photos of outcrops in the Xinlong gold deposit and hand specimens. No. Ⅱ ore body outcrop (a), surface malachite oxide ore of No. Ⅱ ore body (b), Au-Cu 3 outcrop at the southern end of No. Ⅲ ore body (c), surface malachite hand specimen (d), vuggy quartz (e), sparse disseminated pyrite (f), sparse disseminated pyrite (g), pyrophyllite alteration (h), earthy kaolinite in brecciated tetrahedrite ore (i), kaolinite and dense disseminated ore (j), lumpy ore containing tetrahedrite (k) and high-grade lumpy ore (l). Q–quartz; Mal–malachite; Kao–kaolinite; Opl–opal; Td–tetrahedrite.

while the quartz, nevskite, naumannite, and native gold formed at the third stage are paragenetic. They can be distinguished only by microscopic observation in combination with EPMA. Under the microscope, the tetrahedrite cuts through the fractured pyrite (Fig. 5h), and it is visible that the bornite and the tetrahedrite are paragenetic (Fig. 5i). These observations indicate that the tetrahedrite and the bornite formed later than the pyrite. The tetrahedrite formed at the second stage is the best developed, accounting for more than 90% of all metal sulfides in the mining area. The tetrahedrite typically occurs as brecciated, lumpy, or disseminated deposits, and can be further subdivided into zinc-antimony and zinc-arsenite tetrahedrite. The two types of tetrahedrite occur as irregular granular assemblages with a grain size varying from a few tens to a few hundreds of microns and are light olive greenish - brownish gray under the microscope (Figs. 5i–l). They are difficult to distinguish using a microscope but can be distinguished through EPMA (Table 2).

The quartz-nevskite-naumannite-native gold stage is the last stage of the mineralization in the Xinlong gold deposit. As seen under the microscope, the native gold melted out of the naumannite and then filled into the fractures of the tetrahedrite to form semi-enclosed structures (Figs. 5l–m). Native gold also fills into the fractures around the tetrahedrite (Figs. 5j–k), and the nevskite intrudes into the early tetrahedrite and traps the early chalcopyrite (Figs. 5n–o). During this stage, gold mainly occurs in quartz as native gold, which has a golden yellow color and appears irregularly granular under the microscope. With grain sizes varying from a few microns to tens of microns, the native gold is microfine-grained gold (Figs. 5j–m). The EPMA shows that the native gold has gold content of 93.04%–95.55%, indicating high-purity native gold. The naumannite shows a gray reflectance color with a distinct light pink hue (Fig. 5l), with native gold melting locally.

3.5. Metallogenic stages and mineral formation sequence

The metallogenic epochs of the Xinlong gold deposit can

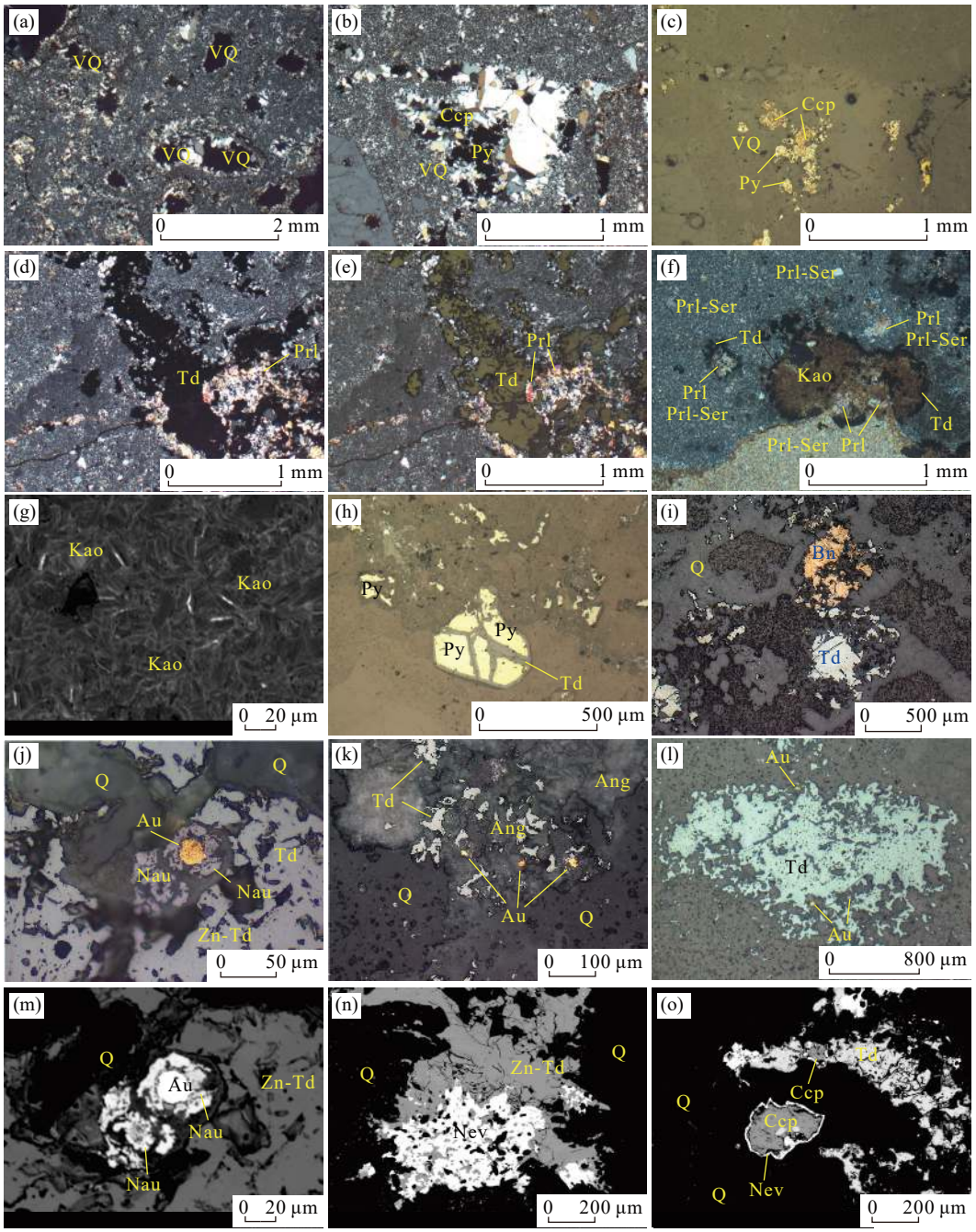

Fig. 5. Microscopic and backscattering photos of ores in the Xinlong gold deposit. VQ–vuggy quartz; Q–quartz; Ccp–chalcopyrite; Py–pyrite; Td–tetrahedrite; Prl–pyrophyllite; Ser–sericite; Kao–kaolinite; Bn–bornite; Ang–anglesite; Nev–nevskite; Zn-Td–zinc-antimony tetrahedrite; Nau–native gold.

be divided into hydrothermal stages I, II and III (Fig. 6) based on the main ore types and the characteristics of mineral assemblages.

Stage I is the early metallogenic stage, during which mainly acidic hydrothermal metasomatism and the leaching of surrounding rocks occurred. As a result, porous quartz and sparsely disseminated pyrite and chalcopyrite generally formed, with weak gold mineralization occurring in the meanwhile.

Stage II was dominated by hydrothermal filling along the staged tectonic fractures or early-formed pores, forming a large number of brecciated, lumpy, and disseminated tetrahedrite mineral series. The mineralization at this stage was largely accompanied by pyrophyllite and kaolinite alteration. This result indicates that the overall pH of the fluids was higher than that in Stage I and that the ore-forming fluids were evolving toward neutrality.

Stage III was slightly later than Stage II and both stages are paragenetic. The ores formed at this stage contain mainly naumannite and nevskite, indicating that the precipitation of a large amount of tetrahedrite formed at Stage II drastically reduced the sulfur fugacity of the hydrothermal fluids, resulting in the independent selenium (Se) precipitation in the ore-forming hydrothermal fluids. Moreover, the ore-forming

Table 1. EPMA data of altered minerals in the Xinlong gold deposit (%).

Sample No.	Tested mineral	SiO_2	Na_2O	Al_2O_3	MgO	K_2O	CaO	P_2O_5	BaO	TiO_2	Total
XL805B-1-1-1	Pyrophyllite	67.30	0.06	28.35	0.03	0.10	0.01	0.02	0.00	0.05	95.92
XL805B-1-1-2	Pyrophyllite	66.98	0.11	29.48	0.04	0.27	0.05	0.04	0.39	0.00	97.36
XL805B-1-1-3	Pyrophyllite	64.93	0.20	29.12	0.04	0.58	0.00	0.00	0.16	0.00	95.03
XL805B-1-1-4	Pyrophyllite	68.48	0.05	28.41	0.03	0.07	0.01	0.00	0.00	0.07	97.12
XL805B-4-1-1	Pyrophyllite	66.63	0.12	28.64	0.01	0.03	0.00	0.00	0.58	0.00	96.01
XL805B-4-1-2	Pyrophyllite	66.58	0.09	28.73	0.03	0.01	0.03	0.00	0.08	0.00	95.55
XL805B-6-1-1	Pyrophyllite	68.08	0.06	28.65	0.06	0.10	0.03	0.04	0.00	0.00	97.01
XL805B-6-1-2	Pyrophyllite	67.09	0.06	28.29	0.03	0.09	0.02	0.01	0.00	0.00	95.58
XL805B-1-2-2	Pyrophyllite	64.76	0.07	27.90	0.10	0.46	0.06	0.00	0.47	0.07	93.89
XL805L-1-Q4-1	Pyrophyllite	65.51	0.16	27.57	0.06	0.36	0.07	0.01	0.52	0.00	94.25
XL805L-1-Q4-2	Pyrophyllite	63.38	0.23	26.29	0.06	0.55	0.08	0.00	0.00	0.00	90.59
XL805L-1-Q4-3	Pyrophyllite	63.87	0.18	27.07	0.07	0.36	0.09	0.03	1.31	0.03	93.00
XL805B-1-1-5	K-bearing aluminosilicate	51.15	0.21	32.90	0.39	6.38	0.11	0.00	0.21	0.01	91.35
XL805B-1- 1-6	K-bearing aluminosilicate	52.50	0.24	35.28	0.44	6.86	0.14	0.00	0.00	0.07	95.52
XL805B-1- 2-1	K-bearing aluminosilicate	58.30	0.22	34.34	0.45	4.92	0.13	0.00	0.52	0.05	98.92
XL805B-1- 2-3	K-bearing aluminosilicate	55.29	0.23	35.73	0.36	6.33	0.09	0.05	0.00	0.07	98.15
XL805L-1-Q1-4	K-bearing aluminosilicate	54.14	0.30	35.71	0.30	6.34	0.07	0.06	0.50	0.03	97.45
XL805L-1-Q1-2	K-bearing aluminosilicate	55.35	0.23	28.25	0.22	5.73	0.06	0.01	0.38	0.05	90.28
XL805L-1-Q1-3	K-bearing kaolinite	48.08	0.16	29.32	0.24	5.94	0.10	0.01	0.04	0.00	83.89
XL805L-1-Q3-1	K-bearing kaolinite	46.50	0.31	32.72	0.47	7.09	0.13	0.05	0.08	0.00	87.34
XL805L-1-Q5-1	K-bearing kaolinite	48.72	0.29	31.41	0.49	6.35	0.25	0.00	0.72	0.00	88.22
XL805L-3-Q1-1	K-bearing kaolinite	43.56	0.14	30.52	0.54	8.59	0.23	0.04	0.00	0.06	83.69

Note: Data are cited from Chen W et al. (2022b). The chemical compositions of target minerals were determined by electron microprobe analysis (EMPA) using a JXA-8230 at the Institute of Mineral Resources, Chinese Academy of Geological Sciences (CAGS) in Beijing.

hydrothermal fluids further evolved to a neutral and low-sulfidation state, which was accompanied by the precipitation of a large amount of gold. Therefore, this stage is the main metallogenic stage of the deposit. Overall, the ore-forming hydrothermal fluids underwent a process in which pH increased and the sulfidation state and sulfur fugacity gradually weakened from the early to the late stage. This process indicates that the ore-forming hydrothermal fluids were subjected to acid-base neutralization and reduction during their migration. In particular, the precipitation of a large amount of tetrahedrite indicates that the ore-forming hydrothermal fluids might have been subjected to strong chemical reduction. The consumption of a large number of sulfur elements created favorable conditions for the precipitation of naumannite, nevskite, and native gold.

4. Genetic types of the Xinlong gold deposit

In the 1980s, Bonham HF (1986) classified epithermal gold deposits into low-sulfidation, high-sulfidation, and alkaline rock types. Heald P et al. (1987) classified them into alunite-kaolinite type (acid sulfate type) and adularia-sericite type, which correspond to the high-sulfidation and low-sulfidation types, respectively. Generally, low-sulfidation deposits contain pyrite-pyrrhotite-arsenopyrite and iron-rich sphalerite; high-sulfidation deposits contain pyrite- enargite-luzonite- covellite, and intermediate-sulfidation deposits generally host a set of intermediate-sulfidation sulfide assemblage consisting of pyrite-tetrahedrite/arsenite tetrahedrite-chalcopyrite and low-iron sphalerite. Compared with gold-rich low-sulfidation deposits, intermediate-sulfidation deposits are rich in Ag and base metals (Hedenquist JW et al., 2000; Jiang SH et al., 2004).

The alteration of the Xinlong gold deposit is dominated by silicification and intermediate to high-grade argillization, which mainly includes pyrophyllite and kaolinite alteration. These altered mineral assemblages are highly similar to the argillization at the periphery of high-sulfidation epithermal gold deposits (Hedenquist JW et al., 2000; Jiang SH et al., 2004). The metallic mineral assemblages in the Xinlong gold deposit are dominated by tetrahedrite mineral series, such as zinc-antimony tetrahedrite, zinc-arsenite tetrahedrite, and iron-arsenite tetrahedrite, followed by nevskite, pyrite, chalcopyrite, bornite, anglesite, native gold, and naumannite (Figs. 6d–l). From a vertical perspective of the ore bodies, these metallic mineral assemblages exhibit similarities to those found in the middle and lower portions of high-

Table 2. EPMA data of ore minerals in the Xinlong gold deposit (%).

Sample No.	Tested mineral	Cu	Zn	As	Se	Ag	Au	Bi	Fe	S	Pb	Te	Sb	Total
XL805B-1-Q1-1	Zinc-antimony tetrahedrite	35.66	5.77	9.91	0.00	0.02	0.04	0.00	1.50	25.67	0.00	0.00	20.90	99.49
XL805B-1-Q1W-2-2	Zinc-antimony tetrahedrite	36.00	5.43	14.00	0.00	0.07	0.00	0.00	1.67	26.35	0.00	0.00	15.06	98.57
XL805L-1-Q1-1S-1	Zinc-antimony tetrahedrite	33.04	5.45	4.58	0.00	0.11	0.00	0.00	1.17	25.21	0.00	0.00	30.62	100.18
XL805L-1-Q3-1S-4	Zinc-antimony tetrahedrite	34.18	5.14	6.89	0.00	0.10	0.00	0.02	1.52	25.35	0.00	0.00	26.42	99.62
XL805B-1-Q4-2-1	Zinc-antimony tetrahedrite	39.98	5.13	9.34	0.00	0.00	0.09	0.00	1.65	26.83	0.00	0.00	16.46	99.47
XL805B-2-Q1-1-2	Zinc-antimony tetrahedrite	38.69	3.74	7.23	0.34	0.00	0.07	0.00	3.35	25.58	0.00	0.00	20.15	99.18
XL805B-2-Q1-2-2	Zinc-antimony tetrahedrite	39.00	3.97	6.64	0.33	0.00	0.06	0.02	3.13	25.82	0.00	0.00	21.50	100.47
XL805B-1-Q3-3	Zinc-antimony tetrahedrite	40.10	5.56	11.37	0.00	0.00	0.08	0.01	1.85	27.24	0.00	0.00	14.25	100.48
XL805B-1-Q1W-1	Zinc-arsenite tetrahedrite	36.89	5.44	15.27	0.00	0.06	0.01	0.00	2.07	27.02	0.00	0.00	11.96	98.72
XL805B-1-Q1W-2-1	Zinc-arsenite tetrahedrite	36.90	5.54	14.71	0.00	0.06	0.00	0.00	1.84	26.61	0.00	0.00	12.10	97.77
XL805B-4-Q1-1	Zinc-arsenite tetrahedrite	43.96	1.73	14.93	0.00	0.00	0.00	0.20	3.54	27.62	0.00	0.00	8.12	100.10
XL805B-6-Q1-1-3	Iron-arsenite tetrahedrite	44.22	0.90	16.67	0.00	0.02	0.00	1.10	4.13	27.85	0.00	0.00	4.25	99.12
XL805B-6-Q1-1-4	Iron-arsenite tetrahedrite	44.08	0.92	17.40	0.00	0.00	0.02	0.98	4.14	27.98	0.00	0.00	3.89	99.41
XL805B-1-Q2-1	Native gold	0.15	0.00	0.00	0.00	3.93	95.28	0.65	0.03	0.05	0.00	0.07	0.00	100.17
XL805L-1-Q2-1S-1	Native gold	0.00	0.02	0.00	0.01	5.44	93.87	0.56	0.02	0.06	0.00	0.00	0.00	99.97
XL805L-1-Q3-1S-1	Native gold	0.00	0.00	0.00	0.00	6.07	93.04	0.48	0.02	0.06	0.00	0.00	0.00	99.68
XL805B-1-Q3-1	Native gold	0.05	0.00	0.00	0.00	3.28	95.55	0.46	0.00	0.01	0.00	0.00	0.00	99.36
XL805B-1-Q3-2	Native gold	0.00	0.00	0.00	0.00	6.65	93.45	0.53	0.00	0.02	0.00	0.15	0.00	100.81
XL805B-1-Q4-2-3	Native gold	0.13	0.00	0.00	0.00	3.43	95.36	0.53	0.04	0.03	0.00	0.17	0.00	99.70
XL805L-3-Q3-1S-1-5	Gold-bearing naumannite	0.40	0.00	0.08	8.32	37.76	51.88	0.17	0.04	0.38	0.00	0.19	0.28	99.50
XL805L-1-Q3-1S-3	Gold-bearing naumannite	0.14	0.00	0.02	7.22	34.00	57.65	0.26	0.11	0.08	0.09	0.00	0.29	99.85
XL805L-3-Q1-1S-1-1	Nevskite	0.30	0.08	0.00	13.87	0.07	0.00	75.38	0.00	8.70	1.04	0.00	1.06	100.50
XL805L-3-Q1-1S-3-1	Nevskite	0.38	0.04	0.00	13.29	0.13	0.01	74.36	0.05	9.37	1.19	0.00	0.93	99.74
XL805B-2-Q1-1-1	Nevskite	0.28	0.00	0.06	16.43	0.01	0.04	60.06	0.01	10.08	1.28	0.00	11.65	99.92
XL805B-2-Q1-2-1	Nevskite	0.32	0.07	0.00	15.44	0.01	0.01	59.37	0.01	10.57	1.50	0.00	11.81	99.13
XL805L-3-Q3-1S-1-1	Chalcopyrite	34.15	0.15	0.00	0.04	0.05	0.04	0.00	30.39	34.72	0.00	0.00	0.00	99.54
XL805L-3-Q3-1S-1-3	Chalcopyrite	34.28	0.04	0.00	0.06	0.03	0.00	0.00	29.97	34.73	0.00	0.30	0.00	99.41
XL805B-1-Q4-2-2	Pyrite	0.00	0.00	0.02	0.03	0.00	0.00	0.00	46.44	53.20	0.00	0.00	0.00	99.71
XL805B-4-Q1-2	Bornite	52.44	0.08	0.00	0.27	0.04	0.24	0.04	13.80	33.03	0.00	0.00	0.00	99.95
XL805B-6-Q1-1-1	Bornite	55.19	0.15	0.00	0.13	0.00	0.08	0.00	12.98	29.70	0.00	1.57	0.00	99.81
XL805B-6-Q1-1-2	Bornite	55.81	0.07	0.00	0.10	0.03	0.02	0.00	12.43	29.61	0.00	1.32	0.00	99.40

Note: Data cited from Chen W et al. (2022b). The test method same as Table 1.

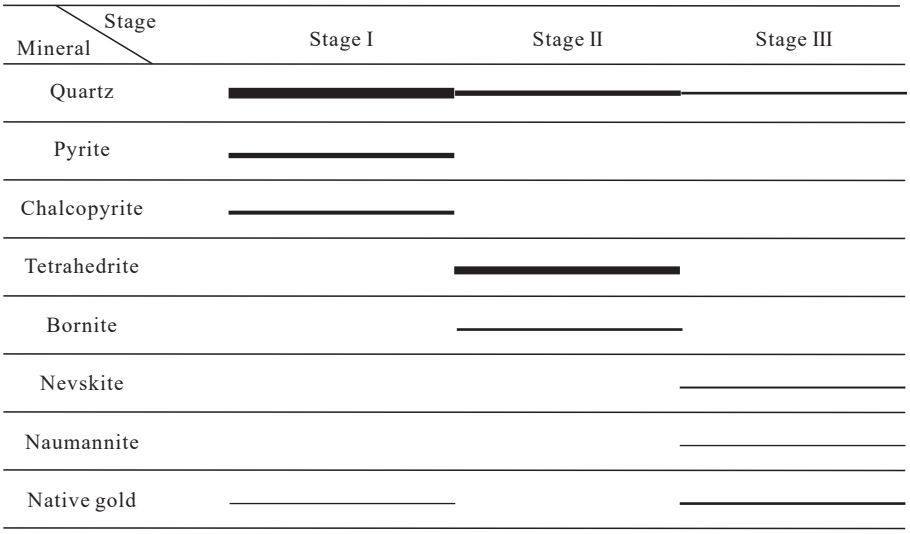

Fig. 6. Paragenesis of main minerals in the Xinlong gold deposit.

sulfidation epithermal gold deposits. For instance, the mineralization in the lower part of the Summitville high-sulfidation epithermal gold deposit in Colorado, USA, is dominated by tetrahedrite (Stoffregen RE, 1987). The selenides are well-developed in the metallic minerals. The enrichment of Se tends to be related to magmatism, and Se is the typomorphic element of many sulfosalt minerals in volcanogenic gold-silver-tin polymetallic deposits (Nekrasov

IY and Lunin SE, 1987; Liu JJ et al., 2020). Overall, it can be inferred that the Xinlong gold deposit is likely a high-sulfidation, epithermal gold deposit of a volcanogenic nature.

5. Significance of the discovery of the Xinlong gold deposit

The Xinlong gold deposit is situated within the central gold mineralized zone of the Lhasa terrane, predominantly occurring in the Longeer-Nyainqentanglha fault-uplift zone located in the central part of the region (Fig. 1). This fault-uplift zone is a notable lithologic boundary, with magmatic rocks on the north side dominated by the volcanic rocks of the Late Jurassic-Early Cretaceous Zenong Group and the magmatic rocks on the south side mainly consisting of volcanic rocks of the Paleogene Linzizong Group (Ma XX et al., 2020). Based on the distribution patterns of the 1∶500000 gold geochemical anomalies of stream sediments in the western segment of the Bangonghu-Nujiang metallogenic belt in Tibet, the gold anomalies are distributed mainly in the volcanic rocks of the Zenong Group near the north side of the fault-uplift zone. In situ apatite U-Pb dating has constrained the age of the Zenong volcanic mining area to 121 ± 5 Ma, which is consistent with the age of the area's Zenong volcanic formation (unpublished data). This indicates a genetic relationship between the two. In fact, the epithermal gold deposit is generally associated with volcanism. Thus, we believe that the volcanic rocks of the Zelong Group have a high potential to host epithermal gold deposits, and it is possible that such deposits exist in the middle Lhasa Terrane. The discovery of the Xinlong gold deposit has presented a novel approach for exploring and prospecting the central gold mineralized zone in the Lhasa terrane, and has introduced new methodologies in the prospecting of rock gold deposits in Northern Tibet.

6. Conclusions

(i) The Xinlong gold deposit was newly discovered during the 1∶50000 mineral geological survey of the central Qinghai-Tibet Plateau by the Institute of Mineral Resources, Chinese Academy of Geological Sciences. The preliminary survey has shown that this gold deposit has favorable metallogenic conditions and a great metallogenic prospect and potential.

(ii) The analysis of the deposit alterations such as silicification, pyrophyllite and kaolinite show that the Xinlong gold deposit is most possibly a high-sulfidation epithermal gold deposit and the first epithermal gold deposit found in Northern Tibet.

(iii) A gold mineralized zone related to Zenong continental volcanic rocks exists in the central part of the Lhasa terrane. The discovery of the Xinlong gold deposit will open a new chapter for the exploration of this gold-mineralized zone.

Acknowledgement

The authors would like to express our gratitude to Academician Jing-wen Mao for his guidance on ore deposit genesis and valuable suggestions for this paper. The authors also thank Director Jian-zhou Yi of the Land and Mineral Rights Trading and Reserve Evaluation Center of Tibet Autonomous Region for his guidance on prospecting directions, and for his long-term help and care. In addition, the authors thank researchers Deng-hong Wang, Shan-bao Liu, Si-hong Jiang, and Shun-da Yuan of the Institute of Mineral Resources, Chinese Academy of Geological Sciences for their guidance and assistance in ore deposit genesis, geochemical anomaly interpretation, mineral prospecting, and mineralogy. The mineralogy and EPMA work were also guided and assisted by Professor De-gao Zhai and Associate Professor Wei Jian of China University of Geosciences (Beijing) and Professor of Senior Engineer Zhen-yu Chen of the Institute of Mineral Resources of the Chinese Academy of Geological Sciences, for which the authors also express our gratitude. Finally, the authors thank anonymous reviewers for their careful and constructive comments. This research was jointly funded by the National Natural Science Foundation of China (41902099), the China Geological Survey Project (DD20230054) and Fundamental Research Funds from the Institute of Mineral Resources and Chinese Academy of Geological Sciences (No. KK2215).

CRediT authorship contribution statement

Wei Chen and Yang Song designed and directed the project; Wei Chen, Yang Song, Qing-ping Liu, Jian-zhen Zhang, Zhuang-zhuang Song, Teng-fei Liu, Qiang Wang, Jia-jia Yu, Yang Li, and Chang Liu carried out the field work; Wei Chen, Miao Sun, and Qing-ping Liu did the EPMA work; Wei Chen wrote the manuscript.

Declaration of competing interest

The authors declare no conflicts of interest.

References

Bonham HF Jr. 1986. Models for volcanic-hosted epithermal precious metal deposits: a review, in International Volcanological Congress, Symposium 5, Hamilton, New Zealand, Proceedings: University of Auckland, Center for Continuing Education, 13–17.

Chen W, Liu TF, Zhang JZ, Liu QP, Song ZZ, Wang Q, Li Q, Zhang YG, Sun M, Liu HZ. 2022a. 1∶50000 mineral geological survey report of Laiduo village and Xinlong (H45E005010, H45E005011) of the Paople's Republic of China. Inernal report (in Chinese with English abstract).

Chen W, Song Y, Liu QP, Zhang JZ, Sun M, Song ZZ, Liu TF, Wang Q, Yu JJ, Li Y, Liu C. 2022b. Discovery and significance of Xinlong gold deposit in southern margin of Bangonghu-Nujiang metallogenic belt. Mineral Deposits, 41(6), 1245–1257 (in Chinese with English abstract).

Fang X, Song Y, Tang JX, Wang JX, Li HF. 2020a. Metallogenic epoch study on the Shangxu gold deposit, Bangong-Nujiang suture zone, Tibet and its geological implications. Acta Geologica Sinica, 94(11), 3376–3390 (in Chinese with English abstract).

Fang X, Tang JX, Beaudoin G, Song Y, Chen YC. 2020b. Geology,

mineralogy and geochemistry of the Shangxu orogenic gold deposit, central Tibet, China: Implications for mineral exploration. Ore Geology Review, 129, 103440. doi: 10.1016/j.oregeorev.2020.103440.

Fang X, Tang JX, Song Y, Beaudoin G, Yang C, Huang XW. 2020c. Genesis of the Shangxu orogenic gold deposit, Bangong-Nujiang suture belt, central Tibet, China: Constraints from H, O, C, Si, He and Ar isotopes. Ore Geology Review, 127, 103810. doi: 10.1016/j.oregeorev.2020.103810.

Gehrels G, Kapp P, Decelles P, Pullen A, Blakey R, Weislogel A, Ding L, Guynn J, Martin A, McQuarrie N, Yin A. 2011. Detrital zircon geochronology of pre-Tertiary strata in the Tibetan-Himalayan orogeny. Tectonics, 30(5), 1–27. doi: 10.1029/2011TC002868.

Geng QR, Peng M, Zhang Z, Guan JL. 2013. Metallogenesis related to magmatic arcs in North and South sides of the Bangong-Nujiang suture in central Tibet. Acta Geologica Sinica, 87(Suppl), 22–24.

Heald P, Foley NK, Hayba DO. 1987. Comparative anatomy of volcanic-hosted epithermal deposits, acid-sulfate and adularia-sericite types. Economic geology, 82(1), 1–26. doi: 10.2113/gsecongeo.82.1.1.

Hedenquist JW, Arribas RA, Gonzalez UE. 2000. Exploration for epithermal gold deposits. Reviews in Economic Geology, 13. doi: 10.5382/Rev.13.07.

Huang HX, Li GM, Liu B, Zhang ZL, Ma D, Qu Z, Xiao WF, Liu H. 2014. Discovery of Shangxu orogenic type gold deposit in northern Tibet and its significance. Mineral Deposits, 33(3), 486–496 (in Chinese with English abstract).

Jiang SH, Nie FJ, Zhang Y, Hu P. 2004. The latest advances in the research of epithermal deposits. Earth Science Frontiers, 11(2), 401–411 (in Chinese with English abstract).

Liu JJ, Zai DG, Wang DZ, Gao S, Yin C, Liu ZJ, Wang JP, Wang YH, Zhang FF. 2020. Classification and mineralization of the Au-(Ag)-Te-Se deposits. Earth Science Frontiers, 27(2), 79–98 (in Chinese with English abstract).

Ma XX, Xu ZQ, Liu F, Zhao ZB, Li HB. 2020. Continental arc tempos and crustal thickening: A case study in the Gangdese arc, southern Tibet. Acta Geologica Sinica, 95(1), 107–123 (in Chinese with English abstract).

Nekrasov IY, Lunin SE. 1987. Conditions for the formation of silver sulfides, selenides and sulfoselenides of the Ag-Sb-S-Se system (as to the experiment data). Mineralogical Magazine, 9, 25–28. doi: 10.3390/min9070430.

Qu XM, Wang RJ, Xin HB, Jiang JH, Chen H. 2012. Age and petrogenesis of A-type granites in the middle segment of the Bangonghu-Nujiang suture, Tibetan plateau. Lithos, 146–147, 264–275. doi: 10.1016/j.lithos.2012.05.006.

Song Y, Tang JX, Qu XM, Wang DH, Xin HB, Yang C, Lin B, Fan SF. 2014. Progress in the study of mineralization in the Bangongco-Nujiang metallogenic belt and some new recognition. Advances in Earth Science, 29(7), 795–809 (in Chinese with English abstract).

Stoffregen RE. 1987. Genesis of acid-sulfate alteration and Au-Cu-Ag mineralization at Summitville. Economic Geology, 82(6), 1575–1591. doi: 10.2113/gsecongeo.82.6.1575.

Tang JX, Duo J, Liu HF, Lang XH, Zhang JS, Zheng WB, Ying LJ. 2012. Minerogenetic series of ore deposits in the East part of the Gangdise metallogenic belt. Acta Geoscientica Sinica, 33(4), 393–410 (in Chinese with English abstract).

Tang JX, Wang Q, Yang C, Ding S, Lang XH, Liu HF, Huang Y, Zheng WB, Wang LQ. 2014. Two porphyry-epithermal deposit metallogenic subseries in Tibetan Plateau: Practice of "absence prospecting" deposit metallogenic series. Mineral Deposits, 33(6), 1151–1170 (in Chinese with English abstract).

Tang JX, Wang Q, Yang HH, Gao X, Zhang ZB, Zou B. 2017. Mineralization, exploration and resource potential of porphyry skarn-epithermal copper polymetallic deposits in Tibet. Acta Geoscientica Sinica. 38(5), 571–613 (in Chinese with English abstract).

Wang CH, Ge LS, Guo XD. 2006. Research on the source of Au in Bengnazangbu placer gold deposit, Tibet. Gold Science and Technology, 14(6), 1–12 (in Chinese with English abstract).

Zhu DC, Li SM, Cawood PA, Wang Q, Zhao ZD, Liu SA, Wang LQ. 2016. Assembly of the Lhasa and Qiangtang terranes in central Tibet by divergent double subduction. Lithos, 245, 7–17. doi: 10.1016/j.lithos.2015.06.023.

Zhu DC, Mo XX, Zhao ZD, Xu JF, Zhou CY, Sun CG, Wang LQ, Chen HH, Dong GC, Zhou X. 2008. Zircon U-Pb geochronology of Zenong Group volcanic rocks in Coqen area of the Gangdese, Tibet and tectonic significance. Acta Petrologica Sinica, 24(3), 401–412 (in Chinese with English abstract).